HelixTrack: Event-Based Tracking and RPM Estimation of Propeller-like Objects

Supplementary Material

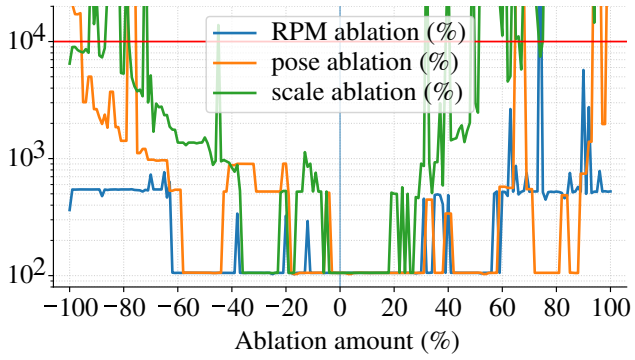

Figure S1. Robustness to initialization errors. We perturb the initial tracker position, in-plane scale, and initial RPM by $\pm\{1, 2, \ldots, 100\}\%$ around the nominal initialization and run HelixTrack end-to-end. For position, we average shifts "toward" and "away from" the nearest distractor (propeller). The plot reports shaft-RPM Mean Absolute Error (MAE) across propellers with MAE ≤ 300 (lower is better); red line marks 10,000 RPM.

S1. Robustness to initialization errors

In this section, we present the figure showing robustness of HelixTrack to initialization errors Fig. S1.

S2. Full Gauss-Newton System with Jacobians

In this section, we describe the full Gauss-Newton System with Jacobians of the terms mentioned in Sec. 3.

Jacobians for all residuals. Let $\sigma(x) = \frac{1}{1+e^{-x}}$ and adopt $\frac{d}{dx}\,\mathrm{wrap}_\pi(x) = 1$ a.e. For polarity,

$$\delta_i = \mathrm{wrap}_\pi(\varepsilon_i^\phi - d_{\mathrm{pol}}), \quad \varepsilon_i^{\mathrm{pol}} = c_{\mathrm{pol}} \sin(\tfrac{1}{2}\delta_i),$$

$$\mathbf{J}_i^{\mathrm{pol}} = c_{\mathrm{pol}} \cdot \tfrac{1}{2} \cos(\tfrac{1}{2}\delta_i)\, \mathbf{J}_i^\phi.$$

For soft band barriers,

$$\varepsilon_i^{\mathrm{in}} = c_b\ \mathrm{softplus}_\tau(r_{\mathrm{in}} - r_i), \quad \varepsilon_i^{\mathrm{out}} = c_b\ \mathrm{softplus}_\tau(r_i - r_{\mathrm{out}}),$$

$$\mathbf{J}_i^{\mathrm{in}} = -c_b\, \sigma\left(\frac{r_{\mathrm{in}} - r_i}{\tau}\right) \mathbf{J}_i^r, \quad \mathbf{J}_i^{\mathrm{out}} = \ c_b\, \sigma\left(\frac{r_i - r_{\mathrm{out}}}{\tau}\right) \mathbf{J}_i^r.$$

Balanced Tip Occupancy (BTO). Define soft occupancies with temperature τ_{occ},

$$m_i^{\mathrm{in}} = \sigma\Big(\frac{r_{\mathrm{in}} - r_i}{\tau_{\mathrm{occ}}}\Big), \quad m_i^{\mathrm{out}} = \sigma\Big(\frac{r_i - r_{\mathrm{out}}}{\tau_{\mathrm{occ}}}\Big),$$

$$p_{\mathrm{in}} = \tfrac{1}{|\mathcal{B}|} \sum_i m_i^{\mathrm{in}}, \quad p_{\mathrm{out}} = \tfrac{1}{|\mathcal{B}|} \sum_i m_i^{\mathrm{out}}.$$

Then

$$\frac{\partial p_{\mathrm{in}}}{\partial \mathbf{q}} = \tfrac{1}{|\mathcal{B}|} \sum_i \Big[-\tfrac{1}{\tau_{\mathrm{occ}}} m_i^{\mathrm{in}}(1 - m_i^{\mathrm{in}}) \mathbf{J}_i^r \Big],$$

$$\frac{\partial p_{\mathrm{out}}}{\partial \mathbf{q}} = \tfrac{1}{|\mathcal{B}|} \sum_i \Big[\tfrac{1}{\tau_{\mathrm{occ}}} m_i^{\mathrm{out}}(1 - m_i^{\mathrm{out}}) \mathbf{J}_i^r \Big].$$

Let

$$\phi(s) = \mathrm{softplus}_\tau(s), \quad \phi'(s) = \sigma(s/\tau),$$
$$\phi''(s) = \sigma(s/\tau)(1 - \sigma(s/\tau))/\tau$$

and

$$s_{\mathrm{in}}^{\mathrm{lo}} = \underline{p_{\mathrm{in}}} - p_{\mathrm{in}}, \quad s_{\mathrm{in}}^{\mathrm{hi}} = p_{\mathrm{in}} - \overline{p_{\mathrm{in}}},$$
$$s_{\mathrm{out}}^{\mathrm{lo}} = \underline{p_{\mathrm{out}}} - p_{\mathrm{out}}, \quad s_{\mathrm{out}}^{\mathrm{hi}} = p_{\mathrm{out}} - \overline{p_{\mathrm{out}}}.$$

Hence

$$\mathbf{J}_{s_{\mathrm{in}}^{\mathrm{lo}}} = -\frac{\partial p_{\mathrm{in}}}{\partial \mathbf{q}},\ \mathbf{J}_{s_{\mathrm{in}}^{\mathrm{hi}}} = \frac{\partial p_{\mathrm{in}}}{\partial \mathbf{q}},\ \mathbf{J}_{s_{\mathrm{out}}^{\mathrm{lo}}} = -\frac{\partial p_{\mathrm{out}}}{\partial \mathbf{q}},\ \mathbf{J}_{s_{\mathrm{out}}^{\mathrm{hi}}} = \frac{\partial p_{\mathrm{out}}}{\partial \mathbf{q}}.$$

Complete GN system. With frozen gates $g_i^\phi = \lambda_\phi w_i^\phi$ and $g_i^r = \lambda_r w_i^r$,

$$\mathbf{H}_{\mathrm{GN}} = \sum_i g_i^\phi (\mathbf{J}_i^\phi)^\top \mathbf{J}_i^\phi + \sum_i g_i^r (\mathbf{J}_i^r)^\top \mathbf{J}_i^r \tag{S1}$$

$$+ \lambda_{\mathrm{pol}} \sum_i (\mathbf{J}_i^{\mathrm{pol}})^\top \mathbf{J}_i^{\mathrm{pol}} \tag{S2}$$

$$+ \lambda_{\mathrm{band}} \sum_i \Big[(\mathbf{J}_i^{\mathrm{in}})^\top \mathbf{J}_i^{\mathrm{in}} + (\mathbf{J}_i^{\mathrm{out}})^\top \mathbf{J}_i^{\mathrm{out}} \Big] \tag{S3}$$

$$+ \lambda_{\mathrm{BTO}} \sum_{q \in \{\mathrm{in,out}\}} \Big[\phi''(s_q^{\mathrm{lo}})\, (\mathbf{J}_{s_q^{\mathrm{lo}}})^\top \mathbf{J}_{s_q^{\mathrm{lo}}} \tag{S4}$$

$$+ \phi''(s_q^{\mathrm{hi}})\, (\mathbf{J}_{s_q^{\mathrm{hi}}})^\top \mathbf{J}_{s_q^{\mathrm{hi}}} \Big] \tag{S5}$$

$$+ \mathbf{H}_{\mathrm{reg}}, \tag{S6}$$

$$\mathbf{g} = \sum_i g_i^\phi\, \varepsilon_i^\phi (\mathbf{J}_i^\phi)^\top + \sum_i g_i^r\, \varepsilon_i^r (\mathbf{J}_i^r)^\top \tag{S7}$$

$$+ \lambda_{\mathrm{pol}} \sum_i \varepsilon_i^{\mathrm{pol}} (\mathbf{J}_i^{\mathrm{pol}})^\top \tag{S8}$$

$$+ \lambda_{\mathrm{band}} \sum_i \Big[\varepsilon_i^{\mathrm{in}} (\mathbf{J}_i^{\mathrm{in}})^\top + \varepsilon_i^{\mathrm{out}} (\mathbf{J}_i^{\mathrm{out}})^\top \Big] \tag{S9}$$

$$+ \lambda_{\mathrm{BTO}} \sum_{q \in \{\mathrm{in,out}\}} \Big[\phi'(s_q^{\mathrm{lo}})\, (\mathbf{J}_{s_q^{\mathrm{lo}}})^\top + \phi'(s_q^{\mathrm{hi}})\, (\mathbf{J}_{s_q^{\mathrm{hi}}})^\top \Big] \tag{S10}$$

$$+ \mathbf{g}_{\mathrm{reg}}. \tag{S11}$$

S3. Dataset Details

This section gives a detailed overview of Timestamped Quadcopter with Egomotion dataset.

The average number of ground-truth timetamps is 4 770, maximum 5 116, minimum 4 906, and median is 4 876.

The average number of processed events is 1.7×10^9, maximum 3.1×10^9, minimum 1.0×10^9, and median is 1.6×10^9.

The average event rate is $60,4 \times 10^6$ (events / second).

In Fig. S2, the aggregated events of the first 10 ms of five 1-second intervals are displayed for all recordings taken at a camera-to-quadcopter distance of 2 m. The intensity of egomotion begins at the top with $M_{\text{ego}} = 1$ and progresses to the last row with $M_{\text{ego}} = 7$. Fig. S3 is structured in the same way and presents recordings for a camera-to-quadcopter distance of 4 m.

S4. AEB-Tracker Parameters Grid Search

As described in Sec. 4.3.1, we first tuned the hyperparameters of the tracker qualitatively. Once a well-performing set of parameters was found on the first 10 milliseconds of the recording, we run the grid search described below.

We performed a comprehensive grid search over four AEB-tracker hyperparameters, 72 combinations in total, evaluated across all recordings and channels. The parameters are as follows.

1. rb (ring_buffer_len): Length of the per-target event/state ring buffers. Larger values smooth estimates more but add inertia,
2. Δt: Integration timestep (seconds) used in the state transition F for (x, y, θ); in particular $\theta \leftarrow \theta + q\ dt$,
3. q_{xy}: Sets both velocity process-noise intensities q_{v_x} and q_{v_y} $[\text{px}^2/\text{s}^3]$. Larger values allow faster changes in velocity (more agility) at the cost of more noise/jitter.
4. q_q: Sets the spin-rate process-noise intensity q_q $[\text{rad}^2/\text{s}^3]$. Larger values let the angular velocity q vary more between updates.

We select the setting that minimizes mean absolute error (MAE). We also report std/median and mean absolute relative error (MArE).

The best configuration observed in Table S4 is $rb = 22$, $\Delta t = 2.5$, $q_{xy} = 5.0$, $q_q = 0.5$, achieving MArE 502.976 and MAE of 38763.807 (aggregated over all recordings and channels).

S5. HelixTrack Parameter and Grid Search

We set the parameters of HelixTrack with a combination of element-wise search and grid search. The complete set of parameters we searched for and their final values are: $q_{\text{jerk}} = 400$, $\lambda_\phi = 1.0$, $\lambda_r = 1.0$, $\lambda_{\text{pol}} = 0.25$, $\lambda_{\text{band}} = 5.0$, $\lambda_{\text{BTO}} = 1.0$, $r_{\text{in}} = 0.2$, $r_{\text{out}} = 1.5$, $\gamma_{\text{tx}} = \gamma_{\text{ty}} = 6.0$, $\gamma_{\text{persp}} = 1.0$. For the complete set of all parameters, not just the ones we searched for, see the attached configuration file and codes.

r_{in}	r_{out}	MAE (RPM) ↓	median
0.0	1.4	25897.838 ± 64560.838	6837.504
0.0	1.5	31173.431 ± 89359.956	6623.163
0.0	1.6	21958.240 ± 62330.271	7017.397
0.0	1.7	33919.799 ± 133795.000	7763.656
0.0	1.8	17984.723 ± 43510.488	6545.428
0.0	1.9	15783.097 ± 43241.885	7078.281
0.1	1.4	4356.810 ± 3985.889	4434.631
0.1	1.5	4814.578 ± 5064.586	4995.041
0.1	1.6	4775.841 ± 3918.283	6323.458
0.1	1.7	4951.189 ± 4428.663	5219.091
0.1	1.8	4687.726 ± 4220.879	5265.247
0.1	1.9	10199.062 ± 39763.741	5339.970
0.2	1.4	10659.736 ± 44302.860	5516.170
0.2	**1.5**	**4052.139 ± 3779.222**	**5200.247**
0.2	1.6	4626.934 ± 3815.512	6050.976
0.2	1.7	4574.203 ± 4136.607	5391.578
0.2	1.8	4691.997 ± 4598.824	5790.502
0.2	1.9	4500.675 ± 3892.523	5436.960
0.3	1.4	6470.363 ± 12126.974	6095.369
0.3	1.5	4401.135 ± 3951.049	5629.956
0.3	1.6	43303.116 ± 274072.299	5758.449
0.3	1.7	4846.586 ± 5777.108	5273.668
0.3	1.8	5826.368 ± 8064.029	5181.593
0.3	1.9	29329.222 ± 179744.825	5588.616

Table S1. Grid search over r_{in} and r_{out} with q_{jerk}=400, λ_ϕ=1.0, λ_{r}=1.0, λ_{pol}=0.25, λ_{band}=5.0, λ_{BTO}=1.0, γ_x=γ_y=6.0, γ_{persp}=1.0. The best setting (lowest MAE mean) is highlighted in bold. See Sec. S5

.

The grid search was performed over r_{in} and r_{out} parameters, results are in Table S1.

The element-wise search was performed with the following set of parameters:

- q_{jerk} (7): 50, 100, 200, 300, 400, 500, 600
- λ_ϕ (2): 0, 1
- λ_r (2): 0, 1
- λ_{pol} (6): 0, 0.25, 0.5, 1, 2, 10
- λ_{band} (5): 0, 1, 5, 10, 20
- λ_{tip} (5): 0, 0.5, 1, 2, 10
- γ_x=γ_y (7): 1, 2, 3, 4, 5, 6, 7
- γ_{persp} (5): 0.01, 0.1, 1, 2, 3

In total, **275** unique experiment configurations were examined, not including the grid search for r_{in} and r_{out}.

S6. Benchmark Complete Results

Across all cells of the Table S3, HelixTrack is consistently the most accurate. It achieves the lowest error in

Figure S2. Aggregated events from all sequences in the Timestamped Quadcopter with Egomotion dataset with camera-to-quadcopter distance of 2 m, from the smallest (top row, M_{ego}=1), to the largest (bottom row, M_{ego}=7) egomotion intensity. Events from the first 10 ms of five 1-second intervals are shown. Positive events displayed in black, negative in gray.

43/52 (MArE), 46/52 (MAE), and 45/52 (RMSE) cases, while AEB-Tracker wins 8/6/5 and DeepEv 1/0/2, respectively. When we compute medians to mitigate heavy-tailed failures, HelixTrack reduces error dramatically relative to AEB-Tracker — MArE: 400.05 $\rightarrow$ 58.95 (-85.3%), MAE: 29,859.50 $\rightarrow$ 5,200.3 (-82.6%), RMSE: 51,662.7 $\rightarrow$ 6,332.25 (-87.7%). DeepEv's medians for MAE/RMSE (14,459.0 / 19,504.4) are below the medians of AEB-Tracker, but its means are much higher due to frequent catastrophic failures.

Effect of distance d. Performance improves with increased camera–scene distance for HelixTrack. At $d = 2\text{m}$ vs. 4m, HelixTrack's medians drop from 63.65 $\rightarrow$ 29.65 (MArE), 5,233.10 $\rightarrow$ 2,697.55 (MAE), and 6,461.30$\rightarrow$3,358.60 (RMSE). Compared to AEB-Tracker, the improvement widens at longer distance: $d = 2\text{m}$: -84.1% / 82.5% / 87.5% (MArE/MAE/RMSE); $d = 4\text{m}$: -94.9% / 94.0% / 95.5%. A plausible explanation is that the propeller occupies a smaller angular extent and generates fewer disruptive events at larger d, which HelixTrack exploits more effectively than the baselines.

Effect of ego-motion magnitude M_{ego}. As motion increases, all methods degrade, but HelixTrack degrades more gracefully. For MAE (medians), HelixTrack stays low for $M_{\text{ego}} = 1 - 3$, and rises for $M_{\text{ego}} = 4 - 7$ — still well below the results of AEB-Tracker. AEB-Tracker shows a pronounced failure at moderate-to-high motion (also reflected in RMSE), while DeepEv exhibits a non-monotonic pattern with moderate medians at certain bins but very heavy tails overall.

Sensitivity to propeller position. The position of a propeller with respect to other propellers / distractors, mat-

Figure S3. Aggregated events from all sequences in the Timestamped Quadcopter with Egomotion dataset with camera-to-quadcopter distance of 4 m, from the smallest (top row, M_{ego}=1), to the largest (bottom row, M_{ego}=7) egomotion intensity. Events from the first 10 ms of five 1-second intervals are shown. Positive events displayed in black, negative in gray.

ters., HelixTrack's easiest configuration is front-left. The most challenging is rear-right, followed by front-right and rear-left. Despite this, HelixTrack still secures the majority of wins in every placement: for example, in front-left it wins 13/13 cells for each metric, and even in rear-right it wins 12/13 (MAE/RMSE) and 11/13 (MArE).

AEB-Tracker collects isolated wins (*e.g.*, low motion with favorable geometry), and DeepEv takes two RMSE cells in specific configurations. However, these wins are not robust: the corresponding 95th percentiles and maxima reveal frequent large errors and outright failures, especially for DeepEv. In contrast, HelixTrack shows low variance in most of the grid.

S7. Loss ablation

The results of the loss term ablation in Table S2 show that removing either the phase-geometry coupling ($\lambda_\phi = 0$) or the radial centering term ($\lambda_r = 0$) leads to failure or order-of-magnitude error increases. For example, at 2 m, $M_{\text{ego}} = 2$, MAE jumps from 90.1 $\pm$ 16.9 (full loss) to 9327.1 $\pm$ 175.7 when $\lambda_r = 0$; at 4 m, $M_{\text{ego}} = 3$ it rises from 3449.3 $\pm$ 3961.3 to 9775.1 $\pm$ 129.5 when $\lambda_r = 0$. Tying the Gauss-Newton pose update to phase residuals r_ϕ and keeping events centered on the blade ring via r_r are important for stabilizing geometry and phase jointly (Sec. 3.5, Eq. 4).

Disabling the soft band-edge barriers ($\lambda_{\text{band}} = 0$) frequently causes failures in the harder settings (average column reports failure; e.g., 2 m, $M_{\text{ego}} = 4$ and 2 m, $M_{\text{ego}} = 7$ both fail), indicating that the annulus constraints are necessary to keep the optimization from leaking inside/outside the informative blade band when background motion and perspective effects are large.

Dropping the polarity term ($\lambda_{\text{pol}} = 0$) degrades the overall average from 4052.1 $\pm$ 2135.0 to 7070.4 $\pm$ 3146.3 and can sharply increase error in challenging cases (e.g., 4 m, $M_{\text{ego}} = 4$: 2152.1 $\pm$ 4126.9 to 8055.4 $\pm$ 1451.6), suggesting that softly aligning polarity clusters with the expected blade edge improves robustness.

Removing BTO ($\lambda_{\text{BTO}} = 0$) changes the overall average

d	M_{ego}	all	$\lambda_\phi = 0$	$\lambda_r = 0$	$\lambda_{\text{pol}} = 0$	$\lambda_{\text{band}} = 0$	$\lambda_{\text{BTO}} = 0$
2 m	1	**92.8 ± 18.4**	98.8 ± 21.5	F	5701.9 ± 3786.9	**92.8 ± 18.4**	92.8 ± 18.4
2 m	2	90.1 ± 16.9	2347.5 ± 2766.6	9327.1 ± 175.7	2103.3 ± 4024.6	**89.7 ± 16.6**	90.1 ± 16.9
2 m	3	680.2 ± 974.9	3883.1 ± 7372.4	8430.9 ± 1589.7	7438.6 ± 1700.5	1319.7 ± 1522.6	**612.5 ± 841.1**
2 m	4	7212.5 ± 332.2	7807.8 ± 3357.2	8720.0 ± 1068.0	7427.7 ± 950.7	F	**6821.1 ± 475.0**
2 m	5	7488.4 ± 2162.5	**6718.4 ± 2246.1**	F	7142.7 ± 1866.7	7452.8 ± 1056.6	8434.2 ± 974.4
2 m	6	7981.4 ± 1705.1	8902.2 ± 307.7	8210.8 ± 2099.4	8182.7 ± 1695.0	7997.8 ± 1939.9	**7868.9 ± 899.4**
2 m	7	**6497.4 ± 1534.1**	F	9194.3 ± 240.5	7873.5 ± 1519.3	F	8032.8 ± 573.4
4 m	1	**1721.3 ± 3263.3**	2176.4 ± 4171.0	9056.5 ± 197.7	F	1783.8 ± 3388.9	2078.1 ± 3976.9
4 m	2	2210.3 ± 4234.0	2319.0 ± 4439.3	9144.2 ± 202.0	4762.0 ± 4837.7	2263.6 ± 4340.8	**1926.3 ± 3666.0**
4 m	3	3449.3 ± 3961.3	4670.2 ± 3608.3	9775.1 ± 129.5	5903.4 ± 4194.7	4409.7 ± 5026.2	**3402.7 ± 3953.5**
4 m	4	**2152.1 ± 4126.9**	4795.1 ± 5431.6	9617.7 ± 224.8	8055.4 ± 1451.6	4582.6 ± 5204.8	2301.9 ± 4426.5
4 m	5	6969.2 ± 4582.9	**5955.7 ± 3973.0**	9573.0 ± 229.7	8630.4 ± 2381.1	6913.1 ± 4549.0	6705.8 ± 4456.2
4 m	6	**6132.8 ± 842.3**	8208.1 ± 1158.6	F	7688.5 ± 623.2	6251.3 ± 2277.5	7990.8 ± 1147.7
Average		**4052.1 ± 2135.0**	F	F	7070.4 ± 3146.3	F	4335.2 ± 1955.8

Table S2. Loss term ablation. Mean Absolute Error (MAE) of RPM (lower is better) under 4-fold cross-validation on the *Timestamped Quadcopter with Egomotion* (TQE) dataset, reported for two camera–target distances (2 m / 4 m) and seven egomotion levels M_{ego}. "All" uses the full batch objective in Eq. (4) with: phase–geometry alignment r_ϕ, radial centering r_r, polarity alignment r_{pol}, soft annulus barriers $r_{\text{in}}, r_{\text{out}}$, and Balanced Tip Occupancy ℓ_{BTO}. Each ablation zeroes the indicated coefficient $(\lambda_\phi, \lambda_r, \lambda_{\text{pol}}, \lambda_{\text{band}}, \lambda_{\text{BTO}})$. TQE ground-truth RPM has $\mu \pm \sigma = 11193.5 \pm 3540.2$. Values are mean ± std.

modestly. This is consistent with BTO's role in discouraging degenerate "only-inside/only-outside" fits rather than driving the solution on its own.

Overall, the *phase* and *radial* data terms provide the backbone for stable pose/phase coupling. The *band* constraints and *polarity* alignment significantly boost robustness under distance and high M_{ego}; and *BTO* offers a small but reliable safety margin against occupancy imbalance. Together, these components are necessary to keep the asynchronous EKF and batched GN updates coherent.

d	M_{ego}	propeller	MArE (%) ↓ ours	MArE (%) ↓ AEB [15]	MArE (%) ↓ DeepEv [4]	MAE (RPM) ↓ ours	MAE (RPM) ↓ AEB [15]	MAE (RPM) ↓ DeepEv [4]	RMSE (RPM) ↓ ours	RMSE (RPM) ↓ AEB [15]	RMSE (RPM) ↓ DeepEv [4]
2 m	1	rear right	**1.3**	61.4	8564.8	**93.7** ✓	5980.8	652423.7	**215.9**	7186.8	785896.2
		rear left	1.3	**0.9**	402.4	81.4 ✓	**73.0**	32090.3	241.4	**241.2**	46466.0
		front left	**1.5**	35.3	4132.0	**118.4** ✓	2487.0	303141.3	**194.1**	3302.9	359054.3
		front right	**1.2**	65.5	94.6	**77.8** ✓	5650.8	8759.2	**186.3**	7673.3	9700.4
	2	rear right	**1.2**	52.1	9523.5	**85.0** ✓	4637.6	749060.3	**178.9**	5549.9	904654.7
		rear left	1.3	**1.2**	4811.7	**87.0** ✓	112.9	357676.3	**277.2**	457.4	455119.6
		front left	**1.5**	49.8	478.5	**114.0** ✓	3075.8	28118.0	**223.5**	3879.2	68394.5
		front right	**1.1**	34.5	7458.3	**74.3** ✓	2035.8	562988.0	**160.9**	3367.3	787219.5
	3	rear right	**1.2**	1198.7	5013.6	**85.1** ✓	102482.5	386360.6	**223.2**	192935.8	437954.9
		rear left	31.7	**15.0**	2059.8	2137.8 ×	**1696.4**	151319.8	4518.8	**3482.9**	184206.2
		front left	**4.2**	467.5	5236.2	**230.2** ✓	37691.4	376231.1	**763.8**	81016.3	448776.7
		front right	**4.8**	1347.9	195.7	**267.9** ✓	110056.2	14595.8	**1031.9**	202948.8	18910.5
	4	rear right	**80.2**	1241.2	12474.4	**7634.3** ×	93995.4	934583.8	**9184.5**	182884.8	1141131.4
		rear left	72.2	**24.5**	8678.3	7135.2 ×	**2828.9**	674615.2	8699.8	**4782.1**	824811.5
		front left	**79.3**	410.3	89.2	**7249.8** ×	29227.1	8417.0	**8825.0**	68684.3	9362.8
		front right	76.3	**59.5**	115.2	6830.5 ×	**5933.1**	9027.6	**8459.0**	11580.7	10408.5
	5	rear right	**62.3**	531.3	106.7	**6347.2** ×	41415.3	9244.0	**7842.7**	79321.0	10241.1
		rear left	**100.9**	480.0	117.9	**9689.7** ×	30491.9	10624.2	**10899.5**	67097.7	12239.0
		front left	**65.0**	389.8	99.3	**5045.3** ×	33458.3	8963.0	**6266.7**	69659.2	9836.3
		front right	**97.7**	1122.0	398.5	**8871.4** ×	77151.0	32523.2	**9710.6**	111267.4	56823.0
	6	rear right	**93.6**	726.2	98.1	**8928.2** ×	56816.8	9461.9	**9874.9**	72370.2	10223.4
		rear left	**97.2**	593.1	108.1	**9221.9** ×	41752.5	9932.7	**10100.1**	56316.4	11232.3
		front left	**89.5**	885.2	103.3	**8283.4** ×	61735.0	9163.9	**9331.8**	72061.8	10279.6
		front right	**57.2**	833.4	96.8	**5492.3** ×	58682.1	8881.7	**6655.9**	72261.9	9697.5
	7	rear right	**72.2**	609.8	10417.8	**7194.7** ×	44713.1	780191.6	**8292.1**	51904.1	894151.1
		rear left	119.1	617.6	**97.0**	**8328.7** ×	45454.3	9180.8	10071.3	51421.3	**10022.4**
		front left	**75.7**	218.3	96.4	**5341.7** ×	16859.6	8811.8	**6817.1**	28904.6	9686.0
		front right	**72.2**	248.4	3638.0	**5124.5** ×	17502.1	253240.6	**6262.9**	29616.6	315329.1
4 m	1	rear right	**73.1**	285.5	834.5	**6616.3** ×	21029.7	57801.3	**8517.8**	46759.1	73901.3
		rear left	**1.2**	57.2	89.6	**76.4** ✓	6038.7	8341.9	**158.4**	20115.0	9422.8
		front left	**1.4**	48.9	88.7	**104.8** ✓	4676.4	7853.7	**255.3**	16769.4	8925.9
		front right	**1.3**	165.4	835.4	**87.8** ✓	13041.8	58054.3	**319.4**	36853.1	74833.5
	2	rear right	91.1	**43.1**	93.1	8561.2 ×	**3847.8**	8671.9	9537.1	**4496.9**	9642.0
		rear left	**1.3**	37.4	3242.1	**85.7** ✓	3529.9	241975.2	**273.2**	5020.2	334534.1
		front left	**1.5**	72.1	93.8	**112.9** ✓	6545.9	8536.3	**254.1**	17753.2	9595.1
		front right	**1.3**	77.3	111.7	**81.4** ✓	4335.3	8969.8	**248.9**	17551.4	10429.0
	3	rear right	70.9	**58.8**	95.8	**5770.0** ×	5904.9	9773.3	**7008.1**	11479.0	10725.7
		rear left	**1.3**	46.8	1801.4	**85.0** ✓	3960.0	140787.4	**211.7**	4845.4	181653.8
		front left	**1.3**	303.1	1937.2	**109.4** ✓	21349.0	146814.9	**210.8**	51357.9	174482.0
		front right	79.8	**39.7**	97.4	7832.8 ×	**4091.3**	9594.5	9394.6	**5306.3**	10465.4
	4	rear right	**83.5**	1194.9	95.2	**8342.3** ×	101987.0	9517.6	**9491.6**	201102.2	10384.6
		rear left	**1.1**	915.1	5251.8	**77.6** ✓	76275.0	426131.2	**222.5**	179370.3	537350.6
		front left	**1.4**	1392.2	389.6	**111.6** ✓	98307.7	26933.9	**288.4**	201185.3	46853.8
		front right	**1.2**	1166.3	13.3	**76.9** ✓	86077.0	693.4	**209.4**	191384.9	2370.2
	5	rear right	**95.3**	994.6	97.8	**9688.6** ×	83816.5	9942.3	**10614.2**	127547.1	10817.5
		rear left	**93.9**	1043.3	94.8	**9316.3** ×	76882.9	9332.0	10400.6	133235.2	**10351.1**
		front left	**1.7**	1092.8	3339.1	**119.1** ✓	81598.8	260136.5	**241.1**	126119.1	310936.4
		front right	**88.3**	1126.9	95.6	**8752.7** ×	93336.6	9351.7	**9711.9**	134050.9	10281.2
	6	rear right	**62.1**	862.2	167.5	**6778.5** ×	68419.4	14322.1	**8015.9**	97991.7	20098.2
		rear left	**57.6**	958.9	3772.0	**5547.2** ×	71680.8	290173.7	**6746.4**	101283.8	359570.3
		front left	**71.5**	995.9	11718.5	**6929.4** ×	76394.7	918479.2	**8522.6**	105034.9	1024071.7
		front right	**60.3**	856.0	130.4	**5276.0** ×	68594.4	12657.2	**6397.8**	102062.7	18155.9

Table S3. Benchmark, Timestamped Quadcopter with Egomotion (TQE). For each presented method and setting (camera-target distance d, egomotion level M_{ego}), the average shaft-RPM mean absolute relative error (MArE), mean absolute error (MAE), and root mean squared error (RMSE) are reported over 4-fold cross-validation across the four propellers (one training propeller per fold). Both AEB-Tracker [15] and DeepEv [4] methods were modified to allow RPM estimation (see Sec. 4.3). TQE ground-truth RPM has $\mu \pm \sigma = 11193 \pm 3540$, min 917, max 15768. $M_{\text{ego}} = 1$ roughly means "slow camera movement", while $M_{\text{ego}} = 5$ means "fast camera movement" (see Fig. 2). As M_{ego} increases, the camera experiences stronger egomotion, leading to increase of the number of events generated in the background.

rb	Δt	q_{xy}	q_q	MArE (%) ↓	median	MAE (RPM) ↓	median
22	2	0.2	0.25	496.419 ± 402.402	428.662	39026.775 ± 35704.452	27149.123
22	2	0.2	0.5	538.978 ± 532.238	335.813	41383.706 ± 40575.234	24252.682
22	2	0.2	1	650.760 ± 610.255	580.914	49669.433 ± 45197.183	44281.303
22	2	0.2	2	697.412 ± 668.144	537.904	53110.765 ± 50873.870	39796.295
22	2	1	0.25	587.555 ± 478.454	411.100	39086.051 ± 29527.280	26570.284
22	2	1	0.5	544.618 ± 510.582	401.498	41860.949 ± 39341.854	30303.074
22	2	1	1	615.645 ± 577.918	553.496	47675.376 ± 44307.127	42378.293
22	2	1	2	694.885 ± 662.955	577.022	52290.860 ± 49815.795	42225.829
22	2	5	0.25	510.618 ± 388.804	397.497	39608.748 ± 29903.648	29931.931
22	2	5	0.5	506.789 ± 472.468	400.054	38952.001 ± 36484.847	29859.506
22	2	5	1	637.420 ± 590.571	597.896	48856.215 ± 44965.901	44515.639
22	2	5	2	664.801 ± 623.023	618.496	50721.102 ± 47445.002	46145.155
22	2.5	0.2	0.25	599.204 ± 405.217	428.662	39154.585 ± 31844.812	27149.123
22	2.5	0.2	0.5	541.204 ± 535.575	335.813	41498.917 ± 40751.855	24252.682
22	2.5	0.2	1	656.356 ± 608.960	626.036	50086.419 ± 45131.954	46723.292
22	2.5	0.2	2	700.457 ± 672.777	537.904	53245.557 ± 51105.783	39796.295
22	2.5	1	0.25	582.944 ± 578.059	404.861	39748.436 ± 29535.466	26218.892
22	2.5	1	0.5	546.194 ± 513.463	401.498	41776.215 ± 39284.539	30303.074
22	2.5	1	1	619.680 ± 584.761	553.496	48030.629 ± 44997.063	42378.293
22	2.5	1	2	696.192 ± 666.004	577.022	52501.734 ± 50255.610	42225.829
22	2.5	5	0.25	511.004 ± 391.626	362.751	39689.789 ± 30294.397	29321.017
22	**2.5**	**5**	**0.5**	**502.976 ± 462.531**	**400.054**	**38763.807 ± 35860.448**	**29859.506**
22	2.5	5	1	635.099 ± 588.028	597.896	48705.017 ± 44782.988	44515.639
22	2.5	5	2	667.087 ± 627.251	618.496	50801.457 ± 47640.824	46145.155
22	3	0.2	0.25	537.926 ± 339.939	388.690	40797.556 ± 25179.970	32766.673
22	3	0.2	0.5	527.948 ± 330.960	482.435	39522.724 ± 23976.905	36248.414
22	3	0.2	1	1572.458 ± 1439.686	1071.014	118593.768 ± 108749.883	77281.079
22	3	0.2	2	1729.390 ± 1080.637	1360.253	130145.474 ± 80259.290	110851.655
22	3	1	0.25	510.972 ± 337.896	387.988	39089.727 ± 25213.444	29948.624
22	3	1	0.5	522.499 ± 311.308	439.585	39133.979 ± 22301.822	32878.498
22	3	1	1	1623.040 ± 1543.883	999.876	122206.230 ± 115777.126	76014.113
22	3	1	2	1819.391 ± 1076.640	1690.690	137646.186 ± 80980.053	131528.893
22	3	5	0.25	528.778 ± 327.504	393.982	39501.077 ± 24184.137	30356.179
22	3	5	0.5	620.653 ± 478.684	477.139	46596.672 ± 35946.071	36226.416
22	3	5	1	1775.582 ± 1666.385	1223.899	133680.214 ± 125213.233	87960.026
22	3	5	2	1868.451 ± 1043.308	1612.597	140173.319 ± 78815.962	128391.421
33	2	0.2	0.25	532.076 ± 542.658	313.137	40817.897 ± 42290.509	23969.480
33	2	0.2	0.5	637.817 ± 621.567	359.301	49911.826 ± 48999.356	28496.135
33	2	0.2	1	722.345 ± 689.412	658.855	54920.949 ± 53254.591	47154.050
33	2	0.2	2	801.631 ± 764.621	785.360	61030.529 ± 59447.827	53700.933
33	2	1	0.25	539.595 ± 519.382	358.879	41270.586 ± 40010.637	28240.227
33	2	1	0.5	628.204 ± 611.694	431.265	48692.147 ± 47599.814	29409.219
33	2	1	1	756.455 ± 724.681	638.275	57933.012 ± 56141.403	47235.750
33	2	1	2	764.616 ± 729.480	607.390	58027.384 ± 56269.086	46369.599
33	2	5	0.25	594.884 ± 547.826	405.281	45212.128 ± 41849.225	29930.397
33	2	5	0.5	610.897 ± 618.423	408.550	47681.510 ± 48051.032	30428.694
33	2	5	1	767.419 ± 722.414	736.989	58523.058 ± 55635.939	54296.780
33	2	5	2	730.990 ± 714.165	662.121	55352.472 ± 55168.873	49709.951
33	2.5	0.2	0.25	543.074 ± 522.441	313.137	41890.431 ± 41373.974	24346.624
33	2.5	0.2	0.5	639.535 ± 619.235	401.370	50020.820 ± 48816.418	30022.854
33	2.5	0.2	1	727.481 ± 698.813	668.252	55288.661 ± 54127.417	47256.535
33	2.5	0.2	2	796.948 ± 755.814	785.360	60555.252 ± 58419.579	53700.933
33	2.5	1	0.25	532.410 ± 506.342	358.879	41036.682 ± 39777.801	28240.227
33	2.5	1	0.5	628.658 ± 612.606	431.265	48665.147 ± 47531.149	29409.219
33	2.5	1	1	743.469 ± 715.875	624.827	57122.147 ± 55425.865	45484.744
33	2.5	1	2	768.513 ± 746.872	601.761	58471.489 ± 57907.022	45485.936
33	2.5	5	0.25	580.653 ± 485.517	490.506	44371.759 ± 38134.757	35223.893
33	2.5	5	0.5	611.000 ± 617.790	408.550	47776.018 ± 48238.017	30428.694
33	2.5	5	1	760.575 ± 742.399	681.596	58266.260 ± 57509.586	48980.242
33	2.5	5	2	727.158 ± 722.614	597.588	54981.420 ± 55610.817	46677.389
33	3	0.2	0.25	780.803 ± 691.614	539.572	56835.266 ± 50675.677	40003.480
33	3	0.2	0.5	711.595 ± 534.618	538.977	52049.844 ± 39029.338	41273.869
33	3	0.2	1	1334.438 ± 1139.468	903.428	98922.204 ± 83349.423	68183.272
33	3	0.2	2	1800.403 ± 1083.555	1388.857	133261.705 ± 80987.728	101892.368
33	3	1	0.25	797.649 ± 670.641	528.780	58814.987 ± 49205.799	37539.753
33	3	1	0.5	752.721 ± 578.674	586.153	56295.285 ± 43346.004	42539.879
33	3	1	1	1371.708 ± 1131.488	885.898	100812.434 ± 83139.604	65690.880
33	3	1	2	1882.050 ± 1109.445	1727.309	138601.952 ± 83147.089	128224.109
33	3	5	0.25	705.389 ± 592.629	559.554	52950.606 ± 43547.516	42432.900
33	3	5	0.5	713.524 ± 573.891	534.925	52982.647 ± 42424.617	39459.804
33	3	5	1	1401.862 ± 1125.218	929.897	102499.465 ± 82047.435	64251.491
33	3	5	2	1843.070 ± 1090.486	1565.962	136415.532 ± 80887.240	122453.756

Table S4. AEB-Tracker grid search results. MAE and MArE reported as $\mu \pm \sigma$. See Sec. S4 for description.